

Uncertainty analysis for the integration of seismic and CSEM data

Myoung Jae Kwon & Roel Snieder, Center for Wave Phenomena, Colorado School of Mines

Summary

Geophysical inverse problems consist of three stages: the forward problem, optimization, and appraisal. We study the appraisal problem for the joint inversion of seismic and controlled source electro-magnetic (CSEM) data and utilize rock-physics models to integrate these two disparate data sets. The appraisal problem is solved by adopting a Bayesian model, and we incorporate four representative sources of uncertainty. These are uncertainties in (1) seismic wave velocity, (2) electric conductivity, (3) seismic data, and (4) CSEM data. Uncertainties in porosity and water saturation are quantified by a posterior random sampling in the model space of porosity and water saturation of a marine one-dimensional structure. We study the relative contributions from four individual sources of uncertainty by performing several statistical experiments. Uncertainties in the seismic wave velocity and electric conductivity play a more significant role on the variation of posterior uncertainty than do uncertainties in the seismic and CSEM data noise. Numerical simulations also show that the assessment of porosity is most affected by uncertainty in seismic wave velocity and the assessment of water saturation is most influenced by uncertainty in electric conductivity. The framework of the uncertainty analysis presented in this study can be utilized to effectively reduce uncertainty of porosity and water saturation derived from integration of seismic and CSEM data.

Introduction

Currently, there is an increasing interest in the integration of the seismic and controlled source electro-magnetic (CSEM) method for deep marine exploration (Harris and MacGregor, 2006). Although the CSEM method has less resolution than the seismic method, it provides additional information about, for example, electric conductivity. Therefore, the CSEM method is considered an effective complementary tool when combined with seismic exploration. The seismic and CSEM methods are disparate exploration techniques that are sensitive to different medium properties. There have been several approaches for joint inversion of disparate data sets (Gallardo and Meju, 2004; Musil et al., 2003). The application of rock-physics models for joint inversion of disparate data sets has recently been studied (Chen et al., 2007). Rock-physics models enable us to interrelate seismic wave velocity and electric conductivity with the reservoir parameters such as porosity, water saturation, or permeability. The main advantage of the approach is that the reservoir parameters have great economic importance. However, the contributions of rock-physics model uncertainties are not yet well understood.

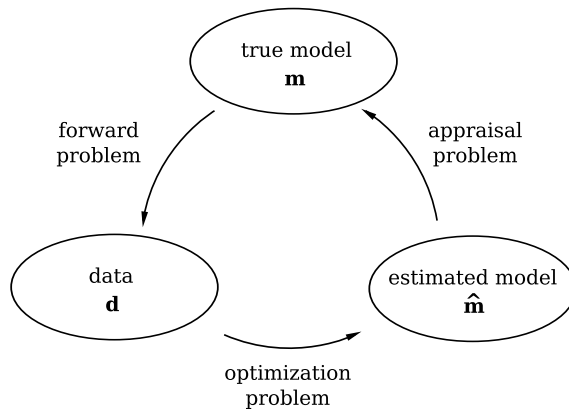


Fig. 1: Division of an inverse problem into a forward problem, an optimization problem, and an appraisal problem (Snieder, 1998).

In many geophysical inverse problems, we have finite data and retrieve a model that has infinitely many degrees of freedom (Snieder, 1998). So far, most geophysical inversion studies have concentrated on finding the model that best fits the data; this is an optimization problem. In this research, we quantify how much confidence we can place in the optimum solution; this is an appraisal problem. The appraisal problem has particular significance when the rock-physics model is used for the joint inversion of the seismic and CSEM data. We investigate the relative contribution of different sources of overall uncertainty that arise when we use rock-physics models for the joint inversion. These include seismic data noise, CSEM data noise, and uncertainties of rock-physics models. We implement several numerical experiments that reflect scenarios we may encounter in practice and compare the uncertainties in the inferred parameters. The comparison reveals the relative contributions of different sources of uncertainty, and we can utilize the procedure to more effectively reduce the uncertainty, depending on whether our interests focus on porosity or water saturation.

Methodology

P -wave velocity (\mathbf{d}_{V_p}) and electric conductivity (\mathbf{d}_{σ_e}) are derived from two reservoir parameters: porosity (\mathbf{m}_ϕ) and water saturation (\mathbf{m}_{S_w}). These reservoir parameters are the target model parameters in this project. Within the Bayesian framework, the prior probabilities of the reservoir parameters are expressed as $\pi_{prior}(\mathbf{m}_\phi)$ and $\pi_{prior}(\mathbf{m}_{S_w})$. There are four possible likelihoods in the Bayesian framework for this project: the likelihoods of the P -wave velocity $f(\mathbf{d}_{V_p}|\mathbf{m}_\phi, \mathbf{m}_{S_w})$, logarithm of electric

Uncertainty analysis for the integration of seismic and CSEM data

conductivity $f(\mathbf{d}_{\sigma_e}|\mathbf{m}_{\phi}, \mathbf{m}_{S_w})$, seismic data $f(\mathbf{d}_s|\mathbf{d}_{V_p})$, and CSEM data $f(\mathbf{d}_e|\mathbf{d}_{\sigma_e})$. Therefore, the posterior probabilities (π_{post}) of the porosity and water saturation are derived from the prior and likelihood probabilities as follows:

$$\begin{aligned}
 & \pi_{post}(\mathbf{m}_{\phi}, \mathbf{m}_{S_w}|\mathbf{d}_{V_p}, \mathbf{d}_{\sigma_e}, \mathbf{d}_s, \mathbf{d}_e) \\
 \propto & \pi(\mathbf{m}_{\phi}, \mathbf{m}_{S_w}, \mathbf{d}_{V_p}, \mathbf{d}_{\sigma_e}, \mathbf{d}_s, \mathbf{d}_e) \\
 = & \pi_{prior}(\mathbf{m}_{\phi})\pi_{prior}(\mathbf{m}_{S_w}) \\
 \times & f(\mathbf{d}_{V_p}|\mathbf{m}_{\phi}, \mathbf{m}_{S_w})f(\mathbf{d}_{\sigma_e}|\mathbf{m}_{\phi}, \mathbf{m}_{S_w}) \\
 \times & f(\mathbf{d}_s|\mathbf{d}_{V_p})f(\mathbf{d}_e|\mathbf{d}_{\sigma_e}). \tag{1}
 \end{aligned}$$

The central limit theorem states that the sum of a sufficiently large number of identically distributed independent random variables follow a normal distribution. This implies that the normal distribution is a reasonable choice for describing probability. Therefore, we assume the priors and likelihoods to follow multivariate Gaussian distribution. If the error structure is apparently different from Gaussian, another appropriate probability function should be modeled. Note that since the forward models employed in this project are nonlinear, the posterior distributions are not necessarily Gaussian.

The posterior model space of this project encompasses porosity and water saturation of several layers. We use a Markov-Chain Monte Carlo (MCMC) sampling method (Kaipio et al., 2000) to indirectly estimate the posterior probability distribution of porosity and water saturation. In this project, the goal of the MCMC sampling method is to retrieve a set of samples, such that the sample distribution describes the joint posterior probability of equation (1). The Metropolis-Hastings algorithm (Hastings, 1970; Metropolis et al., 1953) and Gibbs sampler (Geman and Geman, 1984) are the most widely used samplers for this purpose. We apply the Metropolis-Hastings algorithm for the assessment of posterior probability.

Modeling Procedures

The marine 1-D model employed in this research is shown in Figure 2. The target layer, a gas saturated sandstone layer, is located between shale layers above and below. The soft shale layer is modeled to have the highest clay content and the gas saturated sandstone layer to have the lowest clay content. The mean prior porosity and water saturation values are assumed to be the ground truths.

The bulk modulus is a function of porosity and water saturation. For a fluid-saturated medium, the bulk modulus is given by the Gassmann's equation (Han and Batzle, 2004). We model two phases of pore fluid: water and gas. A mixture of two different pore fluids can be regarded as an effective fluid model, and the bulk modulus is derived from the Wood's equation (Batzle and Wang, 1992). One more factor that has significant effect on the P -wave velocity of a medium is the clay content. Han's empirical relations (Mavko et al., 1998) state that the clay contents reduce the P -wave velocity. In this project, the clay con-

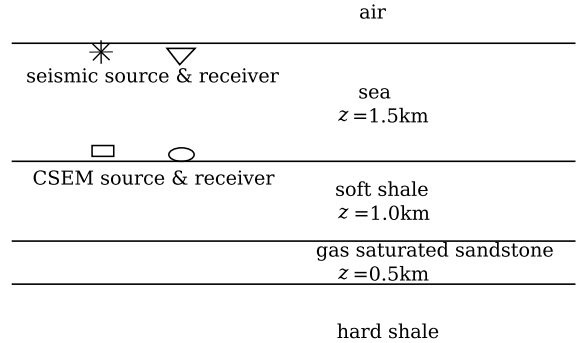


Fig. 2: Cartoon of a marine 1-D model. Seismic source and receiver are located 10 m below the sea surface. CSEM source is located 1 m above the sea bottom and receiver is on the bottom. The earth is modeled as four homogeneous isotropic layers: seawater, soft shale, gas saturated sandstone, and hard shale. The air and hard shale layer are the two infinite half-spaces. The thicknesses (z) of the layers between the two half-spaces are fixed.

tents are assumed to be constant. The electric conductivity in shaley sands is described by the Waxman-Smits formula (Waxman and Smits, 1968). The clay minerals usually have significant cation exchange capacity (CEC), and the variation of the CEC for the different clay mineral is dramatic (Revil et al., 1998). In this project, we simplify the contribution of the clay contents on the electric conductivity and assume that the clay contents in the shale fraction are only composed of kaolinite. We also assume that the distribution of P -wave velocity follows a Gaussian distribution. In contrast, considering that the electric conductivity exhibits exponential variation in most geologic environments, we assume that the electric conductivity follows a lognormal distribution.

Seismic waveform data is synthesized by a ray-tracing algorithm (Docherty, 1987), and we model the primary reflections of P -wave from the top and bottom boundaries of the target sandstone layer. We model the noisy seismic data by adding band-limited noise to the synthesized data. We assume that the seismic data likelihood probability $f(\mathbf{d}_s|\mathbf{d}_{V_p})$ follows multivariate Gaussian distribution. For band-limited noise, the covariance matrix follows from the power spectrum of the bandpass filter. We approximate the covariance matrix of a band-limited noise as the covariance matrix of a white noise. CSEM data is synthesized by a 1-D modeling code (Chave and Cox, 1982), and horizontal electric dipole transmitter and radial electric field response is modeled. The frequency range of the modeling is from 0.1 to 10 Hz. The CSEM noise is categorized as systematic and non-systematic noise. The systematic noise includes the instrument noise and the positioning error. We assume the systematic noise to be proportional to the amplitude of the CSEM signal whereas the non-systematic noise is independent of the signal. We assume the CSEM data likelihood probability $f(\mathbf{d}_e|\mathbf{d}_{\sigma_e})$ to follow a multivariate Gaussian distribution.

Uncertainty analysis for the integration of seismic and CSEM data

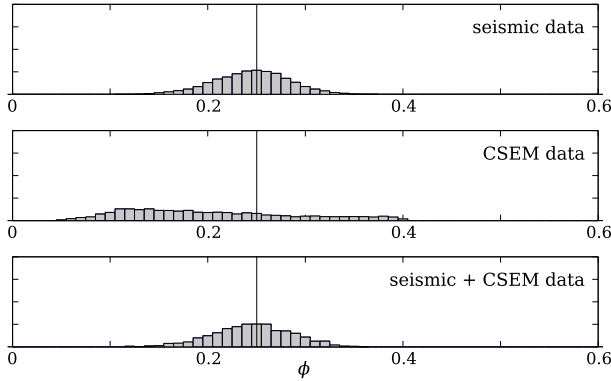


Fig. 3: Histograms of posterior porosity (ϕ) samples of the sandstone layer. Vertical line indicates the ground truth value.

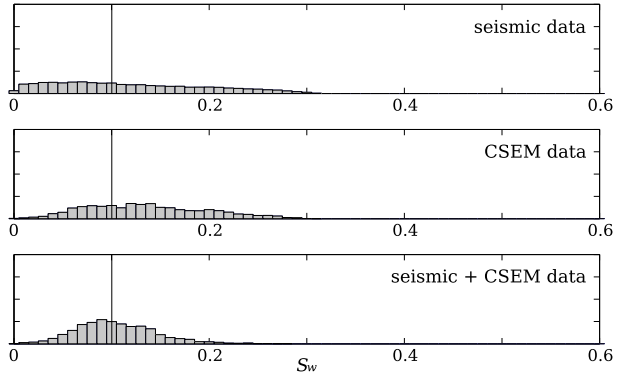


Fig. 4: Histograms of posterior water saturation (S_w) samples of the sandstone layer. Vertical line indicates the ground truth value.

	uncertainty of the individual factors
base level	none of the factors are improved
treatment-1	reducing P -wave velocity uncertainty
treatment-2	reducing electric conductivity uncertainty
treatment-3	reducing seismic data uncertainty
treatment-4	reducing CSEM data uncertainty
treatment-5	reducing P -wave velocity and seismic data uncertainties
treatment-6	reducing electric conductivity and CSEM data uncertainties
improved level	reducing all of the four uncertainty factors

Table 1: Eight numerical experiments for the analysis of the contributions of four possible factors of uncertainty.

Uncertainty Analysis

We perform MCMC sampling to describe the posterior probability distribution. The random sampling is performed within a six dimensional model space that accounts for porosity or water saturation of soft shale, sandstone, and hard shale layers. The posterior distributions of porosity and water saturation of the target sandstone layer are summarized as histograms as shown in Figures 3 and 4. Note that for the employed uncertainty level of rock-physics model and data noise, the histograms show that the single interpretations weakly constrain porosity and water saturation. However, the histograms from the joint interpretation exhibit a narrower sample distribution of porosity and water saturation. The figures also show that the seismic data is more sensitive to porosity than to water saturation, which results from the fact that the P -wave velocity has weaker correlation with water saturation than with porosity. The relatively poor resolution from the CSEM data is attributed to the fact that the sandstone layer is electrically shielded by the more conductive overburden (soft shale layer). These examples illustrate the strength and limitation of both seismic and

CSEM methods and explain the motivation of the joint interpretation of seismic and CSEM data. The histograms from the joint interpretation show smaller posterior uncertainty than do the histograms from the single interpretations. The reduction of uncertainty is more pronounced for water saturation than for porosity.

The posterior uncertainty can generally be assessed by sample mean and sample variance. For the purpose of clarity, we use the Gaussian curves for the representation of the sample mean and sample variance. In this project, we model four factors of uncertainty: uncertainties of the P -wave velocity and electric conductivity, and noise of the seismic and CSEM data. We perform the following numerical experiments to quantify the contributions of the four possible sources of uncertainty. The initial simulation is performed based on a base uncertainty level. For the analysis of the contributions of each of the factors on the posterior uncertainties, six subsequent simulations are performed with reduced uncertainty levels of one or two of the four factors of uncertainty. We perform the last simulation based on reduced uncertainty levels of all factors of uncertainty (improved level). These eight numerical experiments are summarized in Table 1. We compare the posterior distributions from different treatments with the base and improved level and deduce how much a treatment contributes on the overall change of the sample variances. Examples of the posterior distributions of porosity and water saturation are shown in Figures 5 - 6.

Table 2 summarizes the sample variances of posterior probability distributions for the numerical experiments, and Figures 5 and 6 show the posterior probability distributions for the treatments 5 and 6. When we reduce uncertainty levels of one or two uncertainty factors, the resultant posterior distributions exhibit smaller sample variances than the base level, and the sample means generally are closer to the ground truth values. The comparison of the variance values clearly show that reductions of the sample variances of porosity and water saturation are most strongly influenced by the uncertainty of the P -wave velocity and electric conductivity, respectively. The

Uncertainty analysis for the integration of seismic and CSEM data

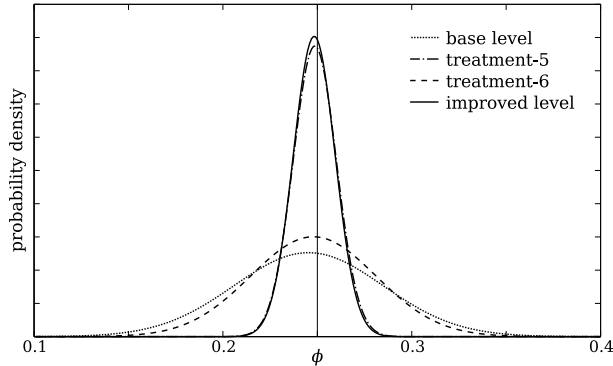


Fig. 5: Posterior probability distributions of porosity ϕ of the sandstone layer. The distributions from the treatments 5 and 6 (Table 1) are compared with those from the base and improved levels. Vertical line indicates the true porosity value.

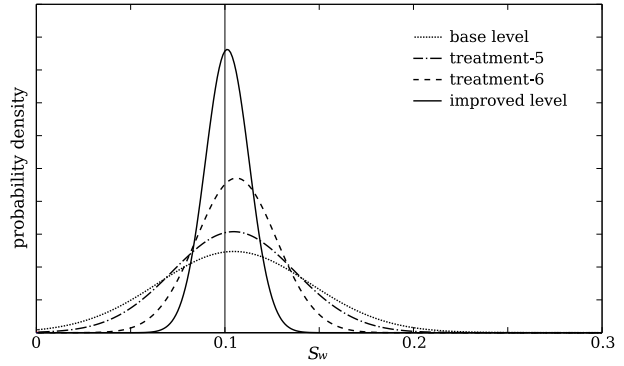


Fig. 6: Posterior probability distributions of water saturation S_w of the sandstone layer. The distributions from the treatments 5 and 6 (Table 1) are compared with those from the base and improved levels. Vertical line indicates the true water saturation value.

sample variance ($\times 10^{-3}$)	$S^2(\phi)$	$S^2(S_w)$
base level	1.56	1.63
treatment-1	0.13	1.38
treatment-2	1.24	0.50
treatment-3	1.19	1.16
treatment-4	1.44	1.27
treatment-5	0.13	1.06
treatment-6	1.11	0.45
improved level	0.12	0.13

Table 2: Sample variances S^2 of porosity ϕ and water saturation S_w of the sandstone layer for the numerical experiments summarized in Table 1.

contributions of the rock-physics model uncertainties on the posterior uncertainties are generally larger than those of the seismic and CSEM data noise. The numerical experiments suggest different ways of accomplishing uncertainty reduction, depending on whether our interests focus on porosity or water saturation. When porosity is our prime concern, we can effectively accomplish uncertainty reduction by an improved rock-physics model describing the P -wave velocity and by suppressing the seismic data noise. On the other hand, if we need more accurate assessment of water saturation, the acquisition of more detailed electric conductivity information and the suppression of CSEM data noise is preferred.

Conclusions

We have shown that the posterior probability random sampling based on the Metropolis-Hastings algorithm is capable of assessing the multi-dimensional probability distribution of porosity and water saturation. We have also shown that the joint inversion of seismic and CSEM data can be achieved by introducing rock-physics models that interconnect the P -wave velocity and electric conductivity. There are four representative sources of uncertainty that influence the posterior probability density of porosity

and water saturation. These uncertainties are related to seismic wave velocity, electric conductivity, seismic data, and CSEM data. Even when single interpretations poorly constrain the posterior distributions of porosity and water saturation, the distributions from joint interpretation are well constrained and exhibit reduced uncertainty.

Assuming two levels of overall uncertainty, we study the relative contributions from four individual sources of uncertainty. The numerical simulations show that rock-physics model uncertainties play a more significant role on the overall uncertainty variation than do uncertainties in the seismic and CSEM data noise. The numerical experiment also suggests different ways of accomplishing uncertainty reduction depending on whether our interests focus on porosity or on water saturation. When porosity is our prime concern, we can effectively accomplish uncertainty reduction by acquiring more precise P -wave velocity information and by suppressing the seismic data noise. On the other hand, if we need a more accurate assessment of water saturation, the acquisition of more detailed electric conductivity information and the suppression of CSEM data noise are desirable.

We emphasize that the conclusions explained above depend on the parameters chosen in this project. Furthermore, there are many sources of uncertainty that we do not take into account such as lithologic variation, variation of mineralogical composition of clay, and depth of layers. The methodology of the uncertainty analysis presented in this project can, however, be extended to a specific problem. The employed method can be used for experimental design and for targeting the source of error that contributes most to posterior uncertainty.

Acknowledgments

We acknowledge the support of the sponsors of Consortium Project at the Center for Wave Phenomena.

Uncertainty analysis for the integration of seismic and CSEM data

References

- Batzle, M. and Z. Wang, 1992, Seismic properties of pore fluids: *Geophysics*, **57**, 1396 – 1408.
- Chave, A. and C. S. Cox, 1982, Controlled electromagnetic sources for measuring electrical conductivity beneath the oceans 1. forward problem and model study: *Journal of Geophysical Research*, **87**, 5327 – 5338.
- Chen, J., G. M. Hoversten, D. Vasco, Y. Rubin, and Z. Hou, 2007, A bayesian model for gas saturation estimation using marine seismic ava and csem data: *Geophysics*, **72**, WA85 – WA95.
- Docherty, P., 1987, Ray theoretical modeling, migration and inversion in two-and-one-half-dimensional layered acoustic media. Ph.D. dissertation: Colorado School of Mines.
- Gallardo, L. A. and M. A. Meju, 2004, Joint two-dimensional dc resistivity and seismic travel time inversion with cross-gradients constraints: *Journal of Geophysical Research*, **109**, B03311.
- Geman, S. and D. Geman, 1984, Stochastic relaxation, gibbs distribution, and the bayesian restoration of images: *IEEE Trans on Pattern Analysis and Machine Intelligence*, **6**, 721 – 741.
- Han, D. and M. Batzle, 2004, Gassmann's equation and fluid-saturation effects on seismic velocities: *Geophysics*, **69**, 398 – 405.
- Harris, P. and L. MacGregor, 2006, Determination of reservoir properties from the integration of csem, seismic, and well-log data: *First Break*, **24**, 53 – 59.
- Hastings, W. K., 1970, Monte carlo sampling methods using markov chains and their applications: *Biometrika*, **57**, 97 – 109.
- Kaipio, J. P., V. Kolehmainen, E. Somersalo, and M. Vauhkonen, 2000, Statistical inversion and monte carlo sampling methods in electrical impedance tomography: *Inverse Problems*, **16**, 1487 – 1522.
- Mavko, G., T. Mukerji, and J. Dvorkin, 1998, *The rock physics handbook*: Cambridge University Press.
- Metropolis, N., A. W. Rosenbluth, M. N. Rosenbluth, and A. H. Teller, 1953, Equation of state calculations by fast computing machines: *The Journal of Chemical Physics*, **21**, 1087 – 1092.
- Musil, M., H. R. Maurer, and A. G. Green, 2003, Discrete tomography and joint inversion for loosely connected or unconnected physical properties: application to crosshole seismic and georadar data sets: *Geophysical Journal International*, **153**, 389 – 402.
- Revil, A., L. M. Cathles, and S. Losh, 1998, Electrical conductivity in shaly sands with geophysical applications: *Journal of Geophysical Research*, **103**, 23925 – 23936.
- Snieder, R., 1998, The role of nonlinearity in inverse problems: *Inverse Problems*, **14**, 387 – 404.
- Waxman, M. H. and L. J. M. Smits, 1968, Electrical conductivities in oil-bearing shaly sands: *Society of Petroleum Engineering Journal*, **8**, 107 – 122.